Doppler Compensation for Optical Inter-Satellite and Satellite-to-Ground Frequency Transfer

Manuele Dassié *German Aerospace Center (DLR), Technical University of Berlin (TUB)*
Gabriele Giorgi, Pablo Nahuel Dominguez, Ludwig Blümel *German Aerospace Center (DLR)*
Christoph Gohle *OHB System AG*

BIOGRAPHY

Manuele Dassié received a B.Sc. in Physics from the University of Fribourg (Switzerland) in 2018, and a M.Sc. in Aerospace Engineering from the Institut Supérieur de l'Aéronautique et de l'Espace in Toulouse (France) in 2020. Manuele is currently a Ph.D. student at Technische Universität Berlin (TUB) and a researcher at the Institute of Communications and Navigation of the German Aerospace Center (DLR) where he works on the synchronization of next-generation satellite systems using optical inter-satellite links.

Gabriele Giorgi received a M.Sc. in Space Engineering from the University of Rome "Sapienza" (Italy) in 2006, and a doctorate in Aerospace Engineering from the Delft University of Technology (the Netherlands) in 2011. He is now a senior researcher at the German Aerospace Center (DLR) in Weßling Oberpfaffenhofen (Germany), where he is involved in the development of technologies and architectures for next generation navigation satellite systems, and a lecturer at the Technical University of Munich (TUM).

Pablo Nahuel Dominguez received his Ph.D. in Experimental Optics at the Ludwig-Maximilians-Universitat in Munich (Germany), after which he joined the company Menlo Systems GmbH. Since June 2021 he is member of the German Aerospace Center (DLR) in Oberpfaffenhofen. His field of interest are optical time and frequency distribution systems and phase stabilization of optical oscillators.

Ludwig Blümel received his diploma degree in microsystems engineering from the University of Applied Sciences in Munich (Germany) in 2005 and his diploma degree in physics from the Ludwig-Maximilians-University in Munich (Germany) in 2013. Since 2019 he works as Scientific Staff at the Institute of Communications and Navigation at the German Aerospace Center (DLR). His fields of interest are optical clocks, time references and optical frequency combs.

Christoph Gohle received his Ph.D. in Physics from the Ludwig-Maximilians-University in Munich (Germany) working on optical frequency combs. He has 18 years of research experience mostly at the Max-Planck-Institute for Quantum Optics in Garching (Germany) working on optical frequency combs, precision spectroscopy and quantum many body physics. He currently works at OHB System AG as a Quantum System Architect on satellite based QKD systems and optical communication in general.

ABSTRACT

Future space missions equipped with optical clocks and terminals for optical inter-satellite links may require syntonization with an accuracy comparable to the stability of typical optical oscillators, 10^{-14} or better. In order to transfer frequency between satellites, and between satellites and the Earth, it is necessary to handle the significant Doppler and Doppler rate effects at the level of several GHz and hundreds of MHz/s, respectively. This paper shows how to estimate the offset between two optical frequency references by taking advantage of the bidirectional capabilities of the optical link, which allows continuous comparison of beat notes (differences between the phase of a locally generated signal and that of a signal received from the other side). Using an approximate knowledge of the position and velocity of the satellites hosting the optical references, we can correct the measurements from the propagation-induced frequency shifts and directly compare the linked clocks, thus retrieving absolute frequency differences. We also show how to mitigate the effect of the measurement noise of the beat notes, which is amplified in the phase-to-frequency transformation. We then evaluate the impact (sensitivity analysis) of the a-synchronicity between the transmission times at the two ends combined with the inaccurate knowledge of position and velocity estimates on the accuracy of the frequency offset determination. Finally, we analyze the rate at which phase measurements must be taken to allow frequency transfer at 10^{-14} accuracy.

I. INTRODUCTION

Free-space optical (FSO) communications have gained significant attention and use in the satellite sector due to improved performance in bandwidth, time and frequency transfer capabilities, inherent robustness against interference and jamming, and lack of bandwidth regulations. Optical inter-satellite links (OISLs) enable direct communication between satellites in space, without the need to retransmit signals through ground stations. This results in lower latency, less dependence on terrestrial infrastructure, and better global coverage for data transmission (Giorgi et al., 2019; Li et al., 2022).

In addition to FSO communications, research is underway to space qualify optical frequency standards that are significantly more stable than currently used atomic clocks operating at microwave frequencies. For example, atomic clocks used in the Galileo system lock onto hyperfine transitions in the microwave regime providing typical frequency stabilities at 10^{-12} for 1 second sampling intervals. Some optical clocks designed for use in space have recently demonstrated a frequency stability of 10^{-15} for averaging times ranging from 1 to 10^4 seconds, exceeding the performance of microwave clocks by several orders of magnitude (Schuldt et al., 2021).

The combination of these two technologies makes it possible to compare very stable frequency standards through bidirectional time and frequency transfer schemes based on optical links. This could result in important contributions to a variety of fields, from orbit determination, navigation, to geodesy and time metrology (Giorgi et al., 2019; Schreiber and Hugentobler, 2013). One field in particular that could benefit greatly from OISLs is that of Global Navigation Satellite Systems (GNSSs), which are essentially constellations of satellites that act as flying clocks transmitting highly accurate timing signals that allow users to determine their position through passive trilateration. Each satellite in the system has its own clock that consists of a frequency reference and a counter, producing a local time scale. For trilateration to work, the time scales of all satellites must be synchronized. This is currently achieved through large networks of ground stations that continuously monitor broadcast signals, which are then used in a sophisticated estimation process to estimate satellite orbits, all offsets between satellite clocks and a time reference (system time), atmospheric parameters, station coordinate deviations, etc. In this approach, satellite orbits and clock deviations produce the same effect on observables and can only be separated and predicted to a certain extent: typical orbit and clock deviation uncertainties transmitted to the end user are in the order of 20-30 centimeters with inter-satellite synchronization at the nanosecond level (Teunissen and Montenbruck, 2017). Future generations of GNSS will instead rely on OISLs to minimize the role of a ground infrastructure in the synchronization process (Giorgi et al., 2019). OISLs enable autonomous inter-satellite clock synchronization at the picosecond level, enabling millimeter-precision inter-satellite ranging. Precise Orbit Determination performance will greatly benefit from the additional observables, with a reduction in Signal in Space Range Error to less than a centimeter, compared to Galileo's few centimeters, providing a much more accurate navigation service to end users (Michalak et al., 2021).

Typically, the synchronization process consists of two steps: first, the clocks are synchronized by exchanging signals to compare their phases using time stamps in a process called Time Transfer (TT). The delay between the time a signal is sent and the time it is received (light propagation time interval) is used to determine the time offset between the clocks, assuming the distance between the two clocks is approximately known. Since the latter is usually not known with high accuracy, Two-Way TT (TWTT) schemes are often used to mitigate the requirement of relative position knowledge (Dassié and Giorgi, 2021). Clocks are then kept synchronized through periodic TWTTs that allow corrections to be determined regularly. The synchronization processes must occur at a sufficiently high rate to prevent the clock phases from diverging too much in-between consecutive TWTT synchronizations.

Another approach to maintaining synchronization is via frequency transfer (FT), in which all clocks have access to the same frequency source, transferred from satellite to satellite via signal exchange, and then each counter integrates this shared frequency to generate timestamps simultaneously (assuming the phases have been aligned at least once with an initial time synchronization event). Future space missions equipped with optical clocks and terminals for optical inter-satellite links might need to syntonize with an accuracy of 10^{-14}, which for a 1064 nanometers laser wavelength translates to an accuracy of approximately 3 Hz. Recently, the German Aerospace Center (DLR) demonstrated the possibility of performing frequency transfer with a stability of 5×10^{-15} at 1 second with a bi-directional optical link established over 10.45 kilometres. The campaign validated the optical terminals design for Lower Earth Orbit (LEO)-to-ground links through the atmospheric channel (Surof et al., 2022).

In order to transfer frequency between satellites and between satellites and ground stations, it is necessary to handle significant Doppler and Doppler rates at the level of several GHz and hundreds of MHz/s, respectively. The objective of this paper is to present a processing scheme that allows FT to be performed aiming at a target of 10^{-14} fractional frequency accuracy with a bidirectional exchange of optical signals.

In Section II, we introduce the two-way optical link model and the relevant quantities we are interested in determining, particularly the frequency offset caused by the inherent instabilities of the frequency references. In this section, we also provide details of the simulation used to evaluate the accuracy of the processing scheme presented in the following sections. In Section III, we present a model of the beat notes (differences between the phase of a locally generated signal and that of a signal received from the other end) that allows us to link the measurements to the aforementioned frequency offset. The Doppler compensation scheme is presented in Section IV. Its goal is the separation of the relative offset from the Doppler and relativistic frequency shifts, leveraging the bi-directional capabilities of the optical link, which allows continuous comparison of measurements obtained at the two ends. Using approximate knowledge of the endpoints' positions and velocities and accurate relativistic models, Doppler shifts can be modelled and removed from the measurements. In a two-way FT, a mis-alignement of measurements taken at the two sides of the transmission and relayed between linked terminals plays a role in amplifying measurement errors and biases. In order to maintain this mis-alignement ot a minimum, two aspects need to be kept under control: the rate of observations should be high enough, and the timestamps of the measurements at the two sides must be synchronized with high accuracy. In Section V we assess the impact (sensitivity analysis) of possible a-synchronicity between the transmission times at the two ends combined with inaccurate knowledge of the position and velocity estimates. In the same section, we analyze the error in the characterization of the relative offset due to the transformation of the measured beat notes (taken in phase) to frequency by numerical derivative method. The minimum rate at which phase measurements must be taken to ensure frequency transfer at the accuracy level of 10^{-14} is also determined.

II. TWO-WAY OPTICAL LINK

Consider two interconnected dynamic endpoints A and B. At each endpoint, an oscillator produces the optical carrier f_0. Because of the inherent instability of the real frequency references, the actual transmitted frequency is slightly different from the nominal frequency, so endpoint A transmits a frequency $f_A(t) = f_0 + \delta f_A(t)$, while B transmits at $f_B(t) = f_0 + \Delta + \delta f_B(t)$, where Δ is the frequency separation, to ensure simultaneous transmission and reception of the signals. Typically we have $\Delta \ll f_0$, so the additional propagation-induced frequency shift due to this term can be considered negligible in the analyses done on the propagation models presented below. For simplicity, in the rest of the paper we will assume $\Delta = 0$ but for practical implementation this quantity must be taken into account. The two frequency references thus have a relative offset $\delta f_{AB}(t) = f_B(t) - f_A(t) = \delta f_B(t) - \delta f_A(t)$. The objective of a frequency transfer is to perform a signal exchange between endpoints and to compare the received signal with the locally generated signal so that this offset can be estimated accurately.

Consider a two-way signal exchange like the one presented in Figure 1, where we have two endpoints N, located at positions $\mathbf{r}_N(t)$ and moving with velocity $\mathbf{v}_N(t) = \frac{d\mathbf{r}_N}{dt}(t)$, $v_N(t) = \|\mathbf{v}_N(t)\|$, $N = A, B$. Each endpoint has access to the local clock, and the two may not be tightly synchronized. Assuming that the intention is to have simultaneous transmission of signals at the two sides, due to de-synchronization the transmission occurs with a slight relative delay (or advance) $t_2 - t_0 = \Delta t_{AB}$. The signal propagates from one satellite to the other with a delay T_{AB} (or T_{BA} for the opposite direction) and finally reception is measured at times t_1 and t_3. The received signals from the two sides are mixed with the locally generated signals, generating a beat signal whose cumulative phase is measured.

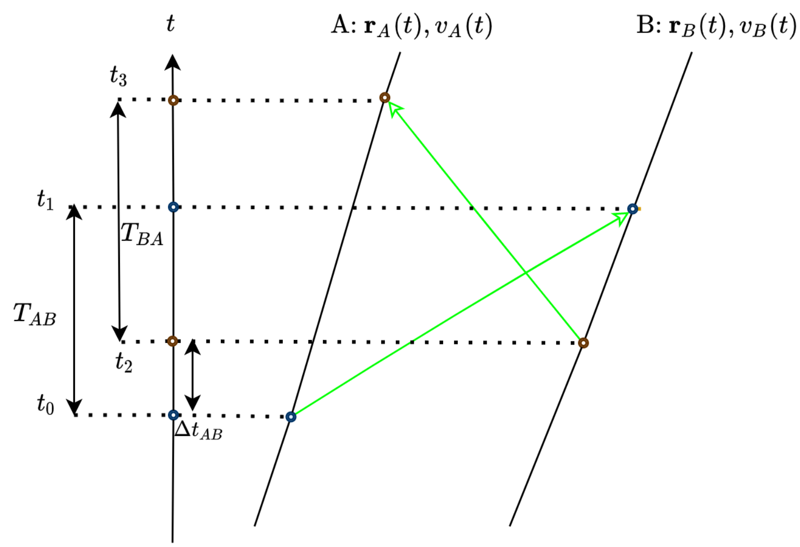

Figure 1: Scheme of transmission and reception of a signal in a two-way exchange.

1. Data simulation

In order to analyze the performance of the frequency transfer scheme presented in this paper, we resort to simulation. A LEO satellite and an Optical Ground Station (OGS) were simulated using the open source General Mission Analysis Tool (GMAT) software, available from NASA (NASA, 2016). The LEO orbit is circular, has a semi-major axis of 6738 kilometres and an inclination of 51.6°. The OGS is located at a latitude of 48°, a longitude of 11° and an altitude of 600 meters. For the analysis,

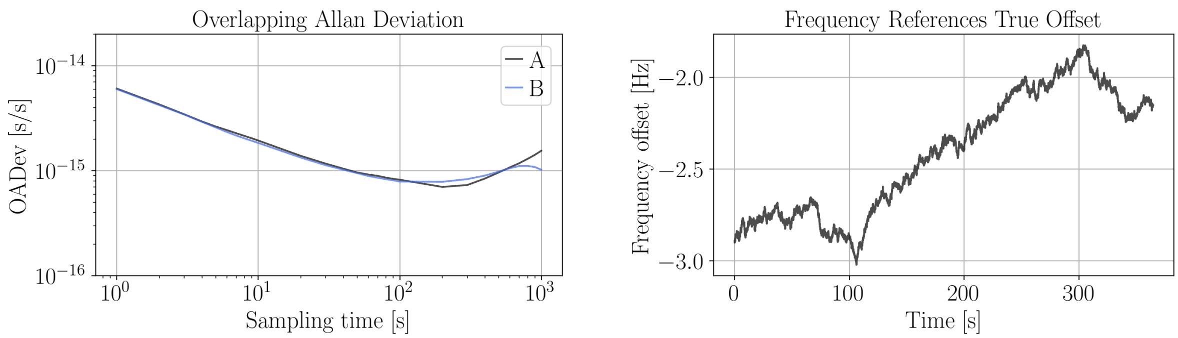

(a) The Overlapping Allan Deviation (Howe et al., 1981), denoted as OADev, of both simulated frequency references.

(b) Time evolution of the frequency offset between the two simulated frequency references.

Figure 2: Stability plot and relative offset of two simulated iodine frequency references with nominal wavelength of 1064 nm.

we considered a satellite pass over the OGS, and the connection between the two end points is considered active only if the elevation angle is higher than 10°. The integration step for propagating the orbit and trajectory of the ground station is 10 ms. Both the OGS and the satellite are equipped with their respective frequency references. These were simulated using a two-state clock model with a simulation time step of 10 ms and show a stability comparable to that of an iodine frequency reference (refer to the stability graph in Figure 2a) whose parameters were determined by fitting measurements of real iodine clocks in the laboratories of the DLR Institute of Communications and Navigation (Schuldt et al. (2021)). We simulated a scenario in which the two clocks have a frequency offset of a few Hz, as visible in Figure 2b.

III. BEAT NOTES OBSERVABLES

Consider the signals measured at endpoint A. Let us momentarily assume that the emitted and received signals have constant frequencies, i.e. both the frequencies generated at the two ends and the frequency shift induced by the propagation are independent of time. The locally generated signal $\left[x_A(t)\right]_A$ can be represented by the following expression:

$$\left[x_A(t)\right]_A = \cos\left(2\pi \left[f_A\right]_A t + \phi_{A0}^{\text{Tx}}\right) \tag{1}$$

In contrast, the received signal, generated at B and measured at A after propagation, is:

$$\left[x_B(t)\right]_A = \cos\left(2\pi \left[f_B\right]_A t + \phi_{A0}^{\text{Rx}}\right) \tag{2}$$

where ϕ_{A0}^{Tx} and ϕ_{A0}^{Rx} are the phase offsets of the respective signals measured at A at time instant $t = 0$. For simplicity of notation, we assume that the two signals have unit amplitude. The notation $\left[\cdot\right]_N$ indicates that the quantity is measured at the end $N = A, B$. Therefore, the frequency $\left[f_A\right]_A$ is the frequency generated by the frequency reference in A and measured locally, and $\left[f_B\right]_A$ is the frequency generated at B and measured at A after propagation.

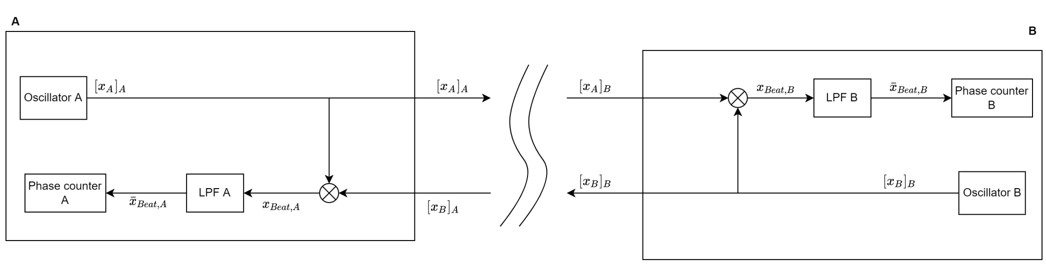

Figure 3: Sketch of the transmitter and receiver processing architectures. At both ends the locally generated and received signals are mixed, low-pass filtered (LPF), and the phase of the resulting signal is measured.

These signals are processed by the receiver according to the scheme in Figure 3. The received signal is mixed with the locally generated signal to generate the signal $x_{Beat,A}(t)$:

$$
\begin{aligned}
x_{Beat,A}(t) &= [x_B(t)]_A \cdot [x_A(t)]_A \\
&= \frac{1}{2}\left[\cos\left(2\pi([f_A]_A + [f_B]_A)t + (\phi^{\text{Tx}}_{A0} + \phi^{\text{Rx}}_{A0})\right) + \cos\left(2\pi([f_B]_A - [f_A]_A)t + (\phi^{\text{Rx}}_{A0} - \phi^{\text{Tx}}_{A0})\right)\right]
\end{aligned}
\tag{3}
$$

where we used the product-to-sum formula for cosines. The mixed signal is then filtered with a low-pass filter (LPF) to remove the first term in (3) and obtain the following signal $\bar{x}_{Beat,A}(t)$:

$$
\begin{aligned}
\bar{x}_{Beat,A}(t) &= \frac{1}{2}\cos\left(2\pi\underbrace{([f_B]_A - [f_A]_A)}_{=f_{Beat,A}}t + \underbrace{(\phi^{\text{Rx}}_{A0} - \phi^{\text{Tx}}_{A0})}_{=\phi_{A0}}\right) \\
&= \frac{1}{2}\cos\left(2\pi f_{Beat,A}t + \phi_{A0}\right)
\end{aligned}
\tag{4}
$$

Introducing the concept of time-dependent frequencies, the raw phase measurements (in cycles) at endpoint A correspond to an initial phase offset plus the cumulative phase over time and some additional noise and bias:

$$
b_A(t) = \frac{\phi_{A0}}{2\pi} + \int_0^t f_{Beat,A}(\tilde{t})d\tilde{t} + \delta b_A(t) + \varepsilon_A(t)
\tag{5}
$$

where $\delta b_A(t)$ is a bias due to unmodeled hardware-related effects or atmospheric delays, and $\varepsilon_A(t) \sim \mathcal{N}(0, \sigma^2_{Beat})$ is a zero-mean additive Gaussian white noise (AWGN) representing measurement noise and other noises arising from platform vibrations, atmospheric propagation, etc.

A similar signal processing is performed at the opposite end, where the following raw phase measurements are taken in B:

$$
b_B(t) = \frac{\phi_{B0}}{2\pi} + \int_0^t f_{Beat,B}(\tilde{t})d\tilde{t} + \delta b_B(t) + \varepsilon_B(t)
\tag{6}
$$

where $\phi_{B0} = \phi^{\text{Rx}}_{B0} - \phi^{\text{Tx}}_{B0}$, $f_{Beat,B}(\tilde{t}) = [f_A]_B(\tilde{t}) - [f_B]_B(\tilde{t})$ and $\varepsilon_B(t) \sim \mathcal{N}(0, \sigma^2_{Beat})$.

So far we have shown how we obtain the measurements $b_A(t)$ and $b_B(t)$. Now we illustrate in detail the model that connects these observables with the quantities we want to separate, namely the offset of the frequency references and the propagation-induced frequency shifts. Consider endpoints A and B in the near-Earth region (on the planet's surface or in orbit) and in relative motion. The theory of general relativity states that two ideal clocks located on the endpoints would tick at different rates, generating the time scales τ_A and τ_B, respectively. Consider the communication scheme presented in Figure 1. Suppose that endpoint A transmits a signal with frequency $[f_A]_A(t) = f_0 + \delta f_A(t)$, while satellite B transmits at $[f_B]_B(t) = f_0 + \delta f_B(t)$. Because of Doppler and relativistic effects, a frequency shift is introduced during the exchange of signals from endpoint A to endpoint B. As shown in (Wolf and Petit, 1995), the expression that relates the received proper frequency $[f_A]_B$ at the time of reception t_1 to the emitted proper frequency $[f_A]_A$ at the time of emission t_0 is as follows:

$$
\frac{[f_A]_B(t_1)}{[f_A]_A(t_0)} = \frac{1 - \frac{\mathbf{n}^T_{AB}\mathbf{v}_{B1}}{c}}{1 - \frac{\mathbf{n}^T_{AB}\mathbf{v}_{A0}}{c}}\left(\frac{d\tau_A}{d\tau_B}\right)_{\text{A=A0,B=B1}}
\tag{7}
$$

where $\frac{d\tau_B}{d\tau_A}$ corresponds to the rate of the proper time of a clock located at endpoint B with respect to the proper time of a clock located in A, $\mathbf{n}_{AB} = \frac{\mathbf{R}_{AB}}{R_{AB}}$ is the line-of-sight (LOS) unit vector, and $\mathbf{R}_{AB} = \mathbf{r}_{B1} - \mathbf{r}_{A0}$. The subscripts $A0$ and $B1$ indicate that the parameters related to the endpoint A should be evaluated at $t = t_0$ and those related to B at $t = t_1$, e.g. $\mathbf{r}_{A0} = \mathbf{r}_A(t_0)$.

The rate term in (7) is:

$$
\begin{aligned}
\left(\frac{d\tau_A}{d\tau_B}\right)_{\text{A=A0,B=B1}} &= \frac{\left(1 + \frac{V_{A0}}{c^2} - \frac{v^2_{A0}}{2c^2}\right)}{\left(1 + \frac{V_{B1}}{c^2} - \frac{v^2_{B1}}{2c^2}\right)} \\
&\approx 1 - \frac{V_{B1} - V_{A0}}{c^2} + \frac{v^2_{B1} - v^2_{A0}}{2c^2}
\end{aligned}
\tag{8}
$$

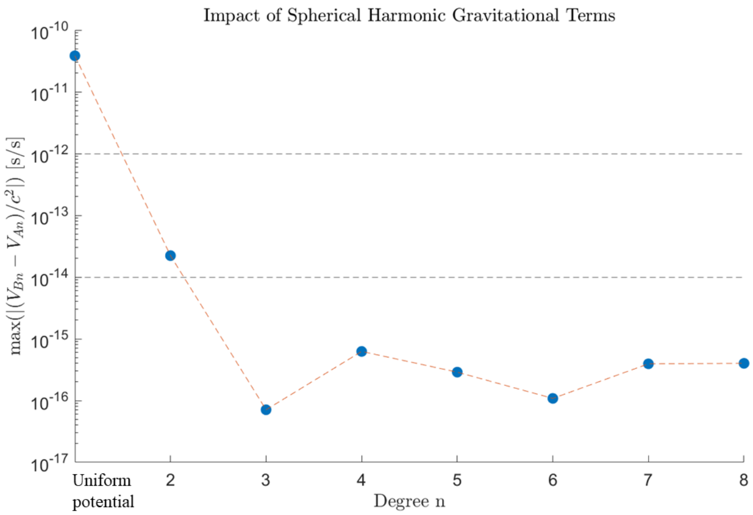

Figure 4: Maximum contribution of the difference $|V_{Bn} - V_{An}|/c^2$ for each geopotential harmonic term of degree n.

where $V_{Nk} = V(\mathbf{r}_{Nk})$ is the gravitational potential at the position of the endpoint $\mathbf{r}_{Nk}$ and v_{Nk} is the magnitude of the endpoint velocity expressed in Earth-Centered-Inertial (ECI) coordinates, $N = A, B$ and $k = 0, 1$. In the second line of (8) we expanded the quotient and kept only the c^{-2} terms. The Earth's gravitational potential $V(\mathbf{r}_N)$ is defined through a summation of spherical harmonics:

$$V(r, \alpha, \beta) = -\frac{GM}{r}\left[1 + \sum_{n=2}^{n_{\max}} \underbrace{\sum_{m=0}^{n} \left(\frac{a_\oplus}{r}\right)^n \bar{P}_{nm}(\sin\beta)\left(\bar{C}_{nm}\cos(m\alpha) + \bar{S}_{nm}\sin(m\alpha)\right)}_{=V_n}\right] \tag{9}$$

where:

- r is radial distance from the Earth's centre;
- G is universal gravitational constant;
- M is Earth's mass;
- $a_\oplus$ is the semi-major axis of the WGS 84 Ellipsoid[1]
- $\bar{C}_{nm}$ and $\bar{S}_{nm}$ are the normalized gravitational coefficients contained in EGM2008[2];
- $\bar{P}_{nm}$ is the normalized associated Legendre function of degree n and order m;
- α and β are respectively the longitude and latitude and of the satellite position in an Earth-Centered-Earth-Fix (ECEF) frame.

As shown in Figure 4, in the specific case of a ground-to-LEO link, where the LEO is at about 400 kilometres altitude and the OGS is at 600 meters altitude, the gravitational potentials V_A and V_B must include the harmonic terms of the geopotential up to the 2nd degree to ensure a frequency transfer at the 10^{-14} level. According to (Dassié and Giorgi, 2021), in this scenario the gravitational influence of any other celestial body in the solar system can be neglected.

Expanding (7) and retaining only c^{-3} terms we obtain:

[1]The World Geodetic System 1984 (WGS 84) represents the best global geodetic reference system for the Earth available at this time for practical applications of mapping, charting, geopositioning, and navigation. This standard includes the definition of the coordinate systems fundamental and derived constants, the ellipsoidal (normal) Earth Gravitational Model (EGM), a description of the associated World Magnetic Model (WMM), and a current list of local datum transformations (National Imagery and Mapping Agency (NIMA), 2000).

[2]An Earth Gravitational Model (EGM) is set of geopotential coefficients used in a spherical harmonic expansion to create a global potential surface to coincide with Mean Sea Level (MSL). A list of coefficients, degrees and orders, with up to 2190 degrees, can be found at (National Geospatial-Intelligence Agency (NGA), 2008).

$$
\begin{aligned}
\frac{[f_A]_B(t_1)}{[f_A]_A(t_0)} \approx 1 &- \frac{V_{AB}}{c^2} + \frac{v_{B1}^2 - v_{A0}^2}{2c^2} - \frac{\dot{R}_{AB}}{c} \\
&+ \frac{V_{AB}}{c^2}\frac{\dot{R}_{AB}}{c} - \frac{v_{B1}^2 - v_{A0}^2}{2c^2}\frac{\dot{R}_{AB}}{c} \\
&- \frac{(\mathbf{n}_{AB}^T\mathbf{v}_{A0})(\mathbf{n}_{AB}^T\mathbf{v}_{B1})}{c^2} + \frac{(\mathbf{n}_{AB}^T\mathbf{v}_{A0})^2}{c^2} \\
&- \frac{(\mathbf{n}_{AB}^T\mathbf{v}_{A0})^2(\mathbf{n}_{AB}^T\mathbf{v}_{B1})}{c^3} + \frac{(\mathbf{n}_{AB}^T\mathbf{v}_{A0})^3}{c^3}
\end{aligned}
\tag{10}
$$

where $V_{AB} = V_{B1} - V_{A0}$ is the difference of the geopotential at B and A at reception and emission instants respectively, and $\dot{R}_{AB} = \mathbf{n}_{AB}^T(\mathbf{v}_{B1} - \mathbf{v}_{A0})$ is the relative velocity projected on the LOS or range rate.

As shown in (10) it is then possible to relate the received frequency to the emitted frequency via:

$$
[f_A]_B(t_1) = [f_A]_A(t_0) + \Delta f_{AB}(t_0, t_1) = f_0 + \delta f_A(t_0) + \Delta f_{AB}(t_0, t_1) \tag{11}
$$

where $\Delta f_{AB}(t_0, t_1)$ includes all the $1/c$ terms in the right-hand side of (10) multiplied by $[f_A]_A(t_0) = f_0 + \delta f_A(t_0)$.

We can therefore characterize the beat frequency in (6):

$$
\begin{aligned}
f_{Beat,B}(t_1) &= ([f_A]_B(t_1) - [f_B]_B(t_1)) \\
&= -\delta f_{AB}(t_0, t_1) + \Delta f_{AB}(t_0, t_1)
\end{aligned}
\tag{12}
$$

where $\delta f_{AB}(t_0, t_1) = ([f_B]_B(t_1) - [f_A]_A(t_0))$.

An analougous expression is derived for the beat frequency at the opposite end:

$$
\begin{aligned}
f_{Beat,A}(t_3) &= ([f_B]_A(t_3) - [f_A]_A(t_3)) \\
&= \delta f_{AB}(t_3, t_2) + \Delta f_{BA}(t_2, t_3)
\end{aligned}
\tag{13}
$$

where $\delta f_{AB}(t_3, t_2) = ([f_B]_B(t_2) - [f_A]_A(t_3))$ and:

$$
\begin{aligned}
\Delta f_{BA}(t_2, t_3) = \Bigg[&-\frac{V_{BA}}{c^2} + \frac{v_{A3}^2 - v_{B2}^2}{2c^2} - \frac{\dot{R}_{BA}}{c} \\
&+ \frac{V_{BA}}{c^2}\frac{\dot{R}_{BA}}{c} - \frac{v_{A3}^2 - v_{B2}^2}{2c^2}\frac{\dot{R}_{BA}}{c} \\
&- \frac{(\mathbf{n}_{BA}^T\mathbf{v}_{B2})(\mathbf{n}_{BA}^T\mathbf{v}_{A3})}{c^2} + \frac{(\mathbf{n}_{BA}^T\mathbf{v}_{B2})^2}{c^2} \\
&- \frac{(\mathbf{n}_{BA}^T\mathbf{v}_{B2})^2(\mathbf{n}_{BA}^T\mathbf{v}_{A3})}{c^3} + \frac{(\mathbf{n}_{BA}^T\mathbf{v}_{B2})^3}{c^3} \Bigg] \times [f_B]_B(t_2)
\end{aligned}
\tag{14}
$$

This time $V_{BA} = V_{A3} - V_{B2}$, $\dot{R}_{BA} = \mathbf{n}_{BA}^T(\mathbf{v}_{A3} - \mathbf{v}_{B2})$ and the subscripts $A3$ and $B2$ indicate that the parameters related to endpoint A have to be evaluated at $t = t_3$ and the ones related to B at $t = t_2$.

As shown in the stability plot in Figure 2a, the frequency references in consideration are stable enough such over the time interval of the exchange (typically shorter than 1 second) the relative frequency offset can be considered constant, $\delta f_{AB}(t_k) \approx \delta f_{AB}(t_0, t_1) \approx -\delta f_{BA}(t_2, t_3)$, $t_k = t_0, \ldots, t_3$. Therefore, we can express the complete model of the observed beat notes (taken in phase) in terms of the quantities we want to estimate:

$$b_A(t) \approx \frac{\phi_{A0}}{2\pi} + \int_0^t \left[\delta f_{AB}(\tilde{t}) + \Delta f_{BA}(\tilde{t} - T_{BA}, \tilde{t})\right] d\tilde{t} + \delta b_A(t) + \varepsilon_A(t) \tag{15}$$

$$b_B(t) \approx \frac{\phi_{B0}}{2\pi} + \int_0^t \left[-\delta f_{AB}(\tilde{t}) + \Delta f_{AB}(\tilde{t} - T_{AB}, \tilde{t})\right] d\tilde{t} + \delta b_B(t) + \varepsilon_B(t) \tag{16}$$

Figure 5 shows an example of the evolution of the quantities $b_A(t)$ and $b_B(t)$ for a Ground-to-LEO link where the signals present an initial phase offset $\phi_{A0} = \phi_{B0} = 0$ rad.

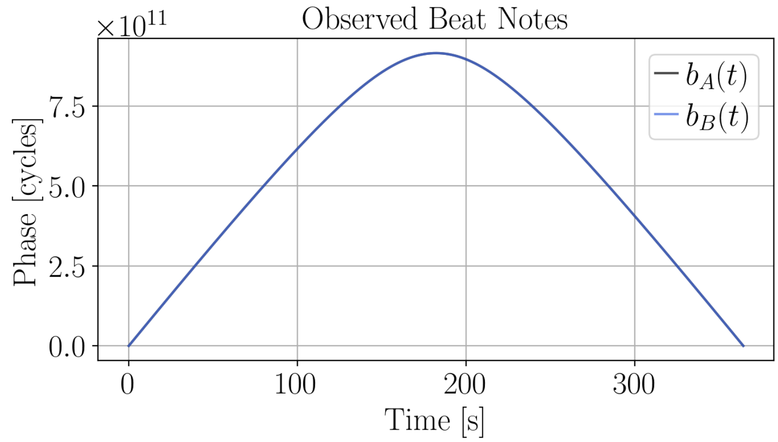

Figure 5: The evolution of $b_A(t)$ and $b_B(t)$ for a Ground-to-LEO link.

IV. THE DOPPLER COMPENSATION ALGORITHM

In the previous Section III we presented how observables are obtained and how they relate to the quantities we want to estimate. In this section we present the procedure to be followed to obtain an estimate of the offset between frequency references by processing the aforementioned measurements.

1. Transformation of phase measurements into frequency values

We are interested in performing a frequency transfer, so from a set of consecutive phase measurements we need to retrieve the respective frequency datapoints. Taking the derivative of (15)-(16) with respect to t we obtain the following:

$$\begin{aligned} z_A(t) &= \frac{d}{dt}\left[b_A(t)\right] = \delta f_{AB}(t) + \Delta f_{BA}(t - T_{BA}, t) + \delta\dot{b}(t) + \dot{\varepsilon}_A(t) \\ z_B(t) &= \frac{d}{dt}\left[b_B(t)\right] = -\delta f_{AB}(t) + \Delta f_{AB}(t - T_{AB}, t) + \delta\dot{b}(t) + \dot{\varepsilon}_B(t) \end{aligned} \tag{17}$$

We can see that if the measurement biases $\delta b_N(t)$ are approximately constant over time, we have that $\delta\dot{b}_N(t) \approx 0$.

In a practical scenario we have access to discrete phase readings at A and B, taken at a rate $r_{meas} = 1/\tau_{meas}$ where τ_{meas} is the sampling interval, so the derivative can only be approximated. The central difference method uses the quotient of the central difference to estimate the derivative at a given point. Such an approximation of the derivative of $b(t)$ at time t is given by (Epperson, 2013):

$$\hat{z}(t, \tau_{meas}) = \frac{b(t + \tau_{meas}) - b(t - \tau_{meas})}{2\tau_{meas}} \tag{18}$$

where $b(t+\tau_{meas})$ and $b(t-\tau_{meas})$ represent the next beat note value measured at time $t+\tau_{meas}$ and the previous measure at time $t-\tau_{meas}$, respectively.

2. Relative frequency offset estimation

It can be assumed that we have access to the approximate positions and velocities of the two communicating endpoints. These parameters can be obtained in several ways (Selvan et al., 2023):

- As for LEO satellites, a GNSS receiver could be placed on board. Typical accuracy of real-time parameters is at the level of meters for position and decimetre per second for velocity. In post-processing, positions can be obtained at the centimetre level and velocities at the millimetre per second level, respectively.
- Doppler Orbitography and Radiopositioning Integrated by Satellite (DORIS) and Satellite Laser Ranging (SLR) are two distinct techniques used for satellite orbit determination. They provide the same level of accuracy as a GNSS receiver, but only in post-processing.
- If the spacecraft under consideration are GNSS satellites, position and velocity data can be obtained by transformation of ephemerides obtained from the predicted orbits provided by the Orbit Determination and Time Synchronization (ODTS) system. These products allow real-time accuracies to be obtained at the decimetre (position) and centimetre per second (velocity) levels.

Using the measurements obtained at the two end points (relayed via the optical links) and the estimated orbital data $(\hat{\mathbf{r}}_A(t), \hat{\mathbf{v}}_A(t))$ and $(\hat{\mathbf{r}}_B(t), \hat{\mathbf{v}}_B(t))$ we can obtain an estimate of the propagation-induced frequency shifts and correct a combination of observables to characterize the offset between frequency references:

$$\delta\hat{f}_{AB}(t) = \frac{1}{2}\left(\hat{z}_A(t,\tau_{meas}) - \hat{z}_B(t,\tau_{meas})\right) - \frac{1}{2}\left(\Delta\hat{f}_{BA} - \Delta\hat{f}_{AB}\right) \tag{19}$$

where $\Delta\hat{f}_{BA} = \Delta f_{BA}(\hat{\mathbf{r}}_{A3}, \hat{\mathbf{v}}_{A3}, \hat{\mathbf{r}}_{B2}, \hat{\mathbf{v}}_{B2})$ and $\Delta\hat{f}_{AB} = \Delta f_{AB}(\hat{\mathbf{r}}_{A0}, \hat{\mathbf{v}}_{A0}, \hat{\mathbf{r}}_{B1}, \hat{\mathbf{v}}_{B1}))$ are the expressions (10)-(14) evaluated with estimates of positions and velocities and $\hat{z}_N(t,\tau_{meas})$ is the approximation of the derivative of the observed beatnotes $b(t)$ obtained via the numerical derivative method (18). It is stressed that the hat notation $\hat{(\cdot)}$ indicates an estimate of the quantity $(\cdot)$. Table 1 shows the order of magnitude of the absolute value of the frequency-normalized half-difference terms.

Table 1: Order of magnitude of each term in $\frac{1}{2f_0}(\Delta f_{BA} - \Delta f_{AB})$ encountered in the Ground-to-LEO link simulation for transmission delays $\Delta t_{AB} = (t_2 - t_0) \in \{0, 0.1\}$ s.

Term	Order of magnitude	
	$\Delta t_{AB} = 0$ s	$\Delta t_{AB} = 0.1$ s
$\frac{1}{2c^2}\left\|V_{BA} - V_{AB}\right\|$	10^{-11}	10^{-11}
$\frac{1}{4c^2}\left\|v_{B1}^2 - v_{A0}^2 - v_{A3}^2 + v_{B2}^2\right\|$	10^{-10}	10^{-10}
$\frac{1}{2c}\left\|\dot{R}_{BA} - \dot{R}_{AB}\right\|$	10^{-10}	10^{-8}
$\frac{1}{2c^3}\left\|V_{AB}\dot{R}_{AB} - V_{BA}\dot{R}_{BA}\right\|$	10^{-16}	10^{-16}
$\frac{1}{2c^3}\left\|(v_{B1}^2 - v_{A0}^2)\dot{R}_{AB} - (v_{A3}^2 - v_{B2}^2)\dot{R}_{BA}\right\|$	10^{-15}	10^{-15}
$\frac{1}{2c^2}\left\|(\mathbf{n}_{BA}^T\mathbf{v}_{B2})(\mathbf{n}_{BA}^T\mathbf{v}_{A3}) - (\mathbf{n}_{AB}^T\mathbf{v}_{A0})(\mathbf{n}_{AB}^T\mathbf{v}_{B1})\right\|$	10^{-16}	10^{-14}
$\frac{1}{2c^2}\left\|(\mathbf{n}_{BA}^T\mathbf{v}_{B2})^2 - (\mathbf{n}_{AB}^T\mathbf{v}_{A0})^2\right\|$	10^{-10}	10^{-10}
$\frac{1}{2c^3}\left\|(\mathbf{n}_{BA}^T\mathbf{v}_{B2})^2(\mathbf{n}_{BA}^T\mathbf{v}_{A3}) - (\mathbf{n}_{AB}^T\mathbf{v}_{A0})^2(\mathbf{n}_{AB}^T\mathbf{v}_{B1})\right\|$	10^{-16}	10^{-16}
$\frac{1}{2c^3}\left\|(\mathbf{n}_{BA}^T\mathbf{v}_{B2})^3 - (\mathbf{n}_{AB}^T\mathbf{v}_{A0})^3\right\|$	10^{-15}	10^{-15}

It turns out that many terms are negligible, in the sense that their contribution is significantly lower than 10^{-14}. Thus, a suitable model for estimating the relative frequency offset with such accuracy is as follows:

$$
\begin{aligned}
\delta \hat{f}_{AB}(t) =& \frac{1}{2}\left(\hat{z}_A(t,\tau_{meas}) - \hat{z}_B(t,\tau_{meas})\right) \\
&+ \frac{f_0}{2c^2}\left(\hat{V}_{BA} - \hat{V}_{AB}\right) && \Delta\text{Term1} \\
&- \frac{f_0}{4c^2}\left(\hat{v}_{A3}^2 - \hat{v}_{B2}^2 - \hat{v}_{B1}^2 + \hat{v}_{A0}^2\right) && \Delta\text{Term2} \\
&+ \frac{f_0}{2c}\left(\dot{\hat{R}}_{BA} - \dot{\hat{R}}_{AB}\right) && \Delta\text{Term3} \\
&+ \frac{f_0}{2c^2}\left((\hat{\mathbf{n}}_{BA}^T\hat{\mathbf{v}}_{B2})(\hat{\mathbf{n}}_{BA}^T\hat{\mathbf{v}}_{A3}) - (\hat{\mathbf{n}}_{AB}^T\hat{\mathbf{v}}_{A0})(\hat{\mathbf{n}}_{AB}^T\hat{\mathbf{v}}_{B1})\right) && \Delta\text{Term4} \\
&- \frac{f_0}{2c^2}\left((\hat{\mathbf{n}}_{BA}^T\hat{\mathbf{v}}_{B2})^2 - (\hat{\mathbf{n}}_{AB}^T\hat{\mathbf{v}}_{A0})^2\right) && \Delta\text{Term5}
\end{aligned} \tag{20}
$$

where each term of the expressions (10) and (14) is evaluated with estimates of positions and velocities.

3. Noise filtering

Suppose the beat observables are measured with an uncertainty $\varepsilon_A(t)$ and $\varepsilon_B(t)$ as presented in (5) and (6). Therefore, in case of perfect knowledge of the positions and velocities of the endpoints, we are able to remove the smooth component and the estimated offset refers to the actual one through:

$$
\delta \hat{f}_{AB}(t) = \delta f_{AB}(t) + \dot{\varepsilon}(t) \tag{21}
$$

where $\dot{\varepsilon}(t) = \frac{1}{2}\left(\dot{\varepsilon}_A(t) - \dot{\varepsilon}_B(t)\right)$. This quantity is the time derivative of a white noise process. In contrast, the frequency reference offset has a large random-walk component, which results from the integration of a white noise process over time. The relation between the Power Spectral Density (PSD) $S_x(\omega)$ of a stochastic process $x(t)$ and the power spectral density $S_{\dot{x}}(\omega)$ of the derivative of $x(t)$ is given by (Barnes and Allan, 1966):

$$
S_{\dot{x}}(\omega) = |\omega|^2 S_x(\omega) \tag{22}
$$

Since white noise has a constant PSD, we can expect the PSD of the offset to be proportional to ω^{-2} and that of the derivative of white noise to be proportional to ω^2. To separate the two components, we can take advantage of the fact that they have different frequency spectra.

We performed a simulation in which the beat notes taken in phase are affected by noise with standard deviation $\sigma_{Beat} = 0.1$ cycles. Figure 6 shows both PSDs of $\delta f_{AB}(t)$ and $\dot{\varepsilon}(t)$. We can see that most of the power of $\delta f_{AB}(t)$ is concentrated in the low frequencies, while the power of the noise $\dot{\varepsilon}(t)$ increases with increasing frequency. From the PSD analysis we can assume that it is possible to isolate the $\delta f_{AB}(t)$ components by filtering the estimated offset with a low-pass filter. A suitable cut-off frequency for the filter would be the intersection of the two lines, i.e., $\omega_C = 2.5$ rad/s.

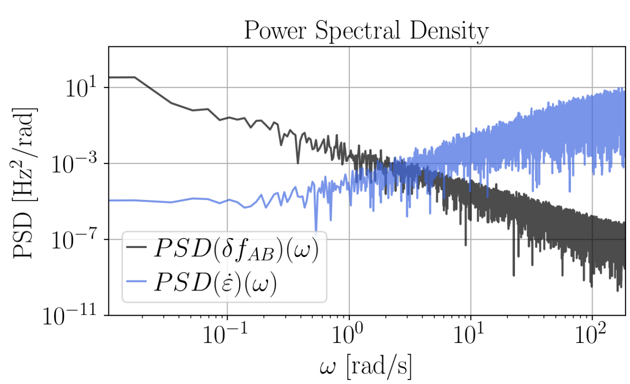

Figure 6: The PSD of the actual frequency reference offset $\delta f_{AB}(t)$ and of $\dot{\varepsilon}(t)$

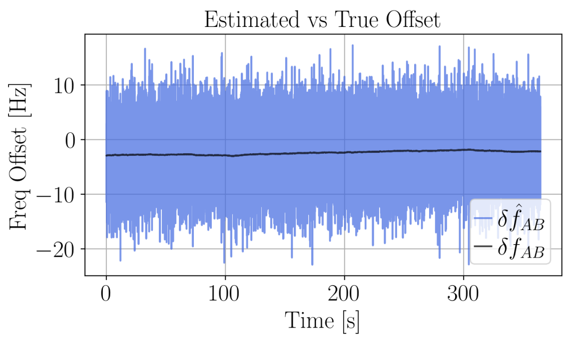

(a) Estimated and actual offset.

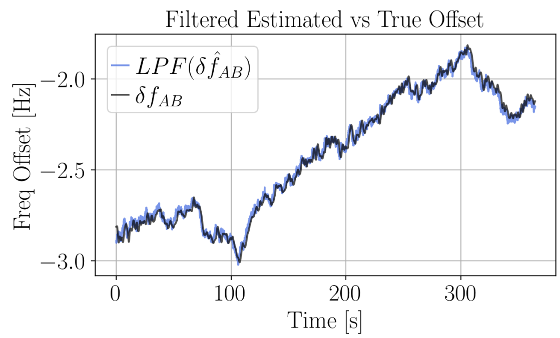

(b) Low-pass filtered estimate and actual offset.

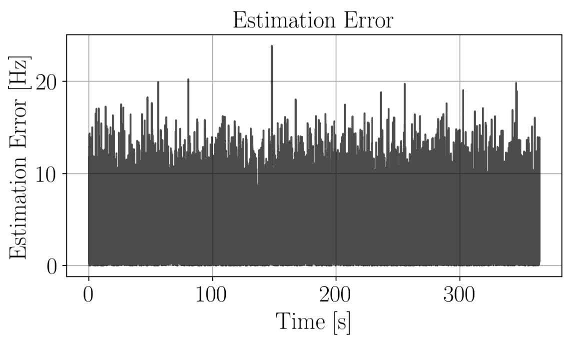

(c) Absolute estimation error $|\delta \hat{f}_{AB} - \delta f_{AB}|$.

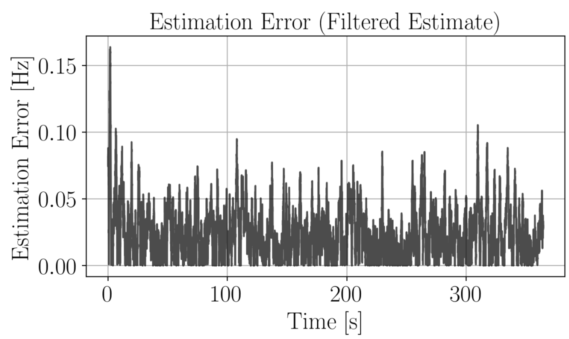

(d) Absolute estimation error $|LPF(\delta \hat{f}_{AB}) - \delta f_{AB}|$.

Figure 7: The evolution of the frequency offset estimate and the low-pass filtered offset estimate versus the actual offset $\delta f_{AB}(t)$ in the situation where the phase observables are noisy ($\sigma_{Beat} = 0.1$ cycles).

Figure 7a shows the actual frequency offset $\delta f_{AB}(t)$ and the estimated offset $\delta \hat{f}_{AB}(t)$ obtained using (20) in the mentioned noisy scenario. We can see that the phase-to-frequency transformation amplifies the effect of measurement noise, leading to an error in the determination of the frequency offset of up to tens of Hz, which is much larger than the desirable threshold of 3 Hz (see Figure 7c). Figure 7b shows the true offset and the filtered low-pass estimate $LPF(\delta \hat{f}_{AB}(t))$ where we used a 5th-order low-pass Butterworth filter with cutoff frequency $\omega_C = 2.5$ rad/s. In Figure 7d, it can be seen that the use of such a filter is very effective and allows the frequency offset to be accurately determined with a maximum error of 0.17 Hz, meeting the accuracy requirements of a maximum error of 3 Hz.

V. SENSITIVITY ANALYSIS

As mentioned previously, we have access to discrete phase measurements and thus transformation to frequency by numerical derivative introduces an approximation error, as does the use of estimates for endpoint positions and velocities, which does not allow a perfect characterization of the bidirectional frequency shift due to propagation. These errors render our offset estimator biased and affect the accuracy with which we can retrieve the offset. In this section we are interested in determining the error margins for position and velocity that allow us to keep these errors below the 10^{-14} threshold and determine the measurement rate that allows us to keep the numerical approximation error below this threshold.

1. Orbital parameters errors

In this section we analyze the sensitivity of the model (20) to orbital parameter errors. In the model, the Doppler components appear as a half-difference, the magnitude of which is significantly smaller than the individual one-way frequency shifts, and by means of subtraction, any quasi-constant error in these components is mitigated, making it easier to obtain accurate estimates of the offset δf_{AB}. Therefore, it is good to ensure that the symmetry in the exchange is maximal. Symmetry can be enhanced by having a simultaneous transmission at the two ends, i.e. $\Delta t_{AB} = t_2 - t_0 = 0$.

An error in satellite velocity would have an impact on the determination of the frequency offset, affecting the terms ΔTerm2,

ΔTerm3, ΔTerm4, and ΔTerm5 of (20). Table 2 shows the velocity error margins for each of these terms and for the transmission delays $\Delta t_{AB} \in \{0, 0.1\}$ s. We assume the LEO satellite is endpoint B, and its velocity esimate is biased by $\delta \mathbf{v}_B = \delta v \mathbf{n}_{AB}$. We consider no velocity error for the OGS (endpoint A). In general, we can see that we have rather generous error margins for velocity biases, with the velocity having to be known to an accuracy of approximately decimetre per second.

Table 2: Velocity error that translates to a frequency transfer errors of 10^{-14} for different transmission delays $\Delta t_{AB} = t_2 - t_0$.

	$\Delta t_{AB} = 0$ s	$\Delta t_{AB} = 0.1$ s
Term	$\lvert\delta v\rvert$ $[m/s]$	
ΔTerm2	0.14	0.14
ΔTerm3	18'000	4
ΔTerm4	91'000	3'800
ΔTerm5	0.14	0.14

A similar sensitivity analysis, on the impact of an error in the position of the satellite on the determination of the frequency offset, is also presented here. Let us assume that the estimated LEO satellite position $\hat{\mathbf{r}}_B(t)$ is affected by an error $\delta \mathbf{r}_B(t)$ in the velocity direction (or along-track since the orbit is circular). The magnitude of the error is assumed to evolve linearly with time:

$$\delta \mathbf{r}_B(t) = \delta r(t) \frac{\mathbf{v}_B(t)}{\|\mathbf{v}_B(t)\|} \tag{23}$$

$$\delta r(t) = \delta r(t_0) + \delta \dot{r}(t_0)(t - t_0) \tag{24}$$

This error would mainly affect the line-of-sight vector determination, in terms ΔTerm3, ΔTerm4 and ΔTerm5 of (20). To simulate the worst case for the error margins of ΔTerm1, which is the term involving the gravitational potential, the position error is considered in the radial direction. Table 3 shows the position error and error rate margins for each one of the aforementioned terms and for different transmission delays Δt_{AB}.

Table 3: Position error and error rate that translates to a frequency transfer error of 10^{-14} for different transmission delays $\Delta t_{AB} = t_2 - t_0$.

	$\Delta t_{AB} = 0$ s		$\Delta t_{AB} = 0.1$ s		
Term	$\lvert\delta r\rvert$ $[m]$	$\lvert\delta \dot{r}\rvert$ $[m/s]$	$\lvert\delta r\rvert$ $[m]$	$\lvert\delta \dot{r}\rvert$ $[m/s]$	Error direction
ΔTerm1	104	47000	104	2100	Radial
ΔTerm3	15	0.26	0.22	0.004	Along-track
ΔTerm4	>100'000	30'000	>100'000	6000	Along-track
ΔTerm5	20	>100'000	20	180	Along-track

It can be seen that for each transmission delay the half-difference of the first-order Doppler terms ΔTerm3 is the most sensitive to position errors, imposing a meter accuracy in position determination and an error rate that should not exceed 26 centimeters per second in the case of simultaneous transmission. It can also be seen that these terms are very sensitive to the transmission delay Δt_{AB}, imposing a decimeter-level accuracy in position determination and a millimetre per second error rate if the transmission is delayed by 0.1 seconds. However, the latter case of relatively low synchronization is very conservative, and even in this case such requirements in orbit knowledge can be met with standard orbit determination techniques.

2. Numerical derivative approximation error

When we calculate the derivative of a function using samples, we must carefully consider the choice of the sampling interval τ_{meas}. If this is chosen too large, the slope of the secant line going through $b(t - \tau_{meas})$ and $b(t + \tau_{meas})$ will be calculated very accurately, but the estimate of the slope of the curve using the secant may be worse. The numerical error introduced by the use of the derivative approximation via (18) translates directly into offset estimation error. In this section we analyze how this error depends on τ_{meas} and determine the maximum sampling interval that allows it to remain below the 10^{-14} threshold.

According to Taylor's theorem, for a small τ_{meas} we have the following:

$$b(t+\tau_{meas}) = b(t) + \frac{db(t)}{dt}\tau_{meas} + \frac{d^2b(t)}{dt^2}\frac{\tau_{meas}^2}{2!} + \frac{d^3b(t)}{dt^3}\frac{\tau_{meas}^3}{3!} + \dots \tag{25}$$

$$b(t-\tau_{meas}) = b(t) - \frac{db(t)}{dt}\tau_{meas} + \frac{d^2b(t)}{dt^2}\frac{\tau_{meas}^2}{2!} - \frac{d^3b(t)}{dt^3}\frac{\tau_{meas}^3}{3!} + \dots \tag{26}$$

Taking the half-difference (25)-(26) we obtain:

$$\frac{db(t)}{dt} = \underbrace{\frac{b(t+\tau_{meas}) - b(t-\tau_{meas})}{2\tau}}_{=\hat{z}(t,\tau_{meas})} - \frac{d^3b(t)}{dt^3}\frac{\tau_{meas}^2}{6} + \dots \tag{27}$$

where in the first term of the right-hand side we identify the approximation of the derivative (18). Thus the numerical error can be expressed as (Epperson, 2013):

$$E(\tau_{meas}) = \hat{z}(t,\tau_{meas}) - \frac{db(t)}{dt} = \frac{d^3b(t)}{dt^3}\frac{\tau_{meas}^2}{6} + \mathcal{O}(\tau_{meas}^4) \tag{28}$$

The algorithm presented in Section IV relies on the processing of a half-difference of $\hat{z}_A(t,\tau_{meas})$ and $\hat{z}_B(t,\tau_{meas})$. Therefore, even in the case of a perfect knowledge of the endpoints' positions and velocities and noiseless measurements, the estimated offset relates to the actual one via:

$$\delta\hat{f}_{AB}(t) = \delta f_{AB}(t) + \frac{1}{2}(E_A(\tau_{meas}) - E_B(\tau_{meas})) \tag{29}$$

In order to keep such error below the 10^{-14} threshold the measurement interval τ_{meas} must satisfy the following conditions:

$$\frac{1}{2}|E_A(\tau_{meas}) - E_B(\tau_{meas})| < 3\,Hz \iff \tau_{meas} < \sqrt{\frac{12 \times 3\,Hz}{\max|\frac{d^3}{dt^3}[b_A(t)] - \frac{d^3}{dt^3}[b_B(t)]|}} \approx 0.6\,s \tag{30}$$

where we used $\max|\frac{d^3}{dt^3}[b_A(t)] - \frac{d^3}{dt^3}[b_B(t)]| \approx 100$ Hz/s^2 obtained by deriving the curves in Figure 5 three times. We can see that if we want to process the half-difference of the beat notes, we need to have a beat note phase measurement rate in the order of 1.6 Hz. This is not a stringent requirement to meet.

VI. CONCLUSION

This work focused on how to accurately estimate the frequency offset between two highly dynamic frequency references, such as those that might be linked between satellites or satellite and ground, with an accuracy better than 10^{-14} via a two-way frequency transfer scheme.

In Section II, we presented the two-way optical link model and the relevant quantities we are interested in determining, particularly the frequency offset between the references.

In Section III, we characterized the observables obtained in a typical frequency transfer experiment. These are phase measurements, which correspond to the difference between the phases of a locally generated signal and that received from the opposite end. The model of the observables links them to the quantities we want to separate, i.e., the stochastic relative frequency offset and the smooth propagation-induced frequency shift. We then presented a 10^{-14} accurate model of the propagation-induced frequency shift that includes the Doppler shift and relativistic effects. It is shown, for example, that the modeling of the Earth's geopotential must consider harmonics up to the J_2 moment.

In Section IV we presented the procedure to be followed to obtain an estimate of the offset between frequency references from the observables. As a first step, it is shown how to transform phase measurements into frequency values via a numerical derivation scheme, the central difference method. Next, an expression is presented for an estimate of the frequency offset that is based on a combination of the measurements obtained at both ends and approximate knowledge of the positions and velocities of both endpoints. Finally, an approach is presented to filter out the measurement noise that is amplified during the phase-to-frequency transformation. Exploiting the different spectral characteristics of the derivative of the measurement noise and of the offset we can use of a low pass filter to effectively estimate the latter.

For a 10^{-14} accuracy in the frequency offset estimation, it is necessary to keep the errors on the endpoints' positions and velocities below a certain threshold. The error margins on these parameters were calculated and presented in Section V. Depending on the transmission delay, position errors vary from meter- to decimeter-level. The position error rate should not exceed few millimeters per second. Error margin on the velocity parameter are more generous, allowing errors up to a decimeter per second. Finally, an analysis of the impact of the error arising from numerical derivation on the determination of the offset allowed the measurement rate to be determined: this should be larger than 1 Hz.

This work shows that with a bidirectional exchange a 10^{-14} frequency transfer scheme is not only fundamentally feasible, but can also be implemented in practice. By having syntonized clocks and assuming that the constant offset due to initialization of counters at different times is characterized at least once, we can maintain clock synchronization by continuous frequency adjustments.

ACKNOWLEDGEMENTS

We acknowledge support from the European Space Agency via the Optical Clock Comparison and Range Rate Unit (OCCRU) project.

REFERENCES

Barnes, J. and Allan, D. (1966). A statistical model of flicker noise. *Proceedings of the IEEE*, 54(2):176–178.

Dassié, M. and Giorgi, G. (2021). Relativistic modelling for accurate time transfer via optical inter-satellite links. *Aerotecnica Missili & Spazio*.

Epperson, J. F. (2013). *An Introduction to Numerical Methods and Analysis*. Wiley Publishing, 2nd edition.

Giorgi, G., Schmidt, T. D., Trainotti, C., Mata-Calvo, R., Fuchs, C., Hoque, M. M., Berdermann, J., Furthner, J., Günther, C., Schuldt, T. D., Sanjuan, J., Gohlke, M., Oswald, M., Braxmaier, C., Balidakis, K., Dick, G., Flechtner, F., Ge, M., Glaser, S., König, R., Michalak, G., Murböck, M., Semmling, M., and Schuh, H. (2019). Advanced technologies for satellite navigation and geodesy. *Advances in Space Research*, 64(6):1256–1273.

Howe, D., Allan, D., and Barnes, J. (1981). Properties of signal sources and measurement methods. In *Thirty Fifth Annual Frequency Control Symposium*, pages 669–716.

Li, R., Lin, B., Liu, Y., Dong, M., and Zhao, S. (2022). A survey on laser space network: Terminals, links, and architectures. *IEEE Access*, 10:34815–34834.

Michalak, G., Glaser, S., Neumayer, K., and König, R. (2021). Precise orbit and earth parameter determination supported by LEO satellites, inter-satellite links and synchronized clocks of a future GNSS. *Advances in Space Research*.

NASA (2016). General mission analysis tool (gmat) v.r2016a. `https://software.nasa.gov/software/GSC-17177-1`.

National Geospatial-Intelligence Agency (NGA) (2008). Egm2008 - wgs 84 version. `https://earth-info.nga.mil/GandG/wgs84/gravitymod/egm2008/egm08_wgs84.html`.

National Imagery and Mapping Agency (NIMA) (2000). World Geodetic System 1984. Its Definition and Relationships with Local Geodetic Systems. Technical report, US Department of Defense, 3rd Ed.

Schreiber, K. U. and Hugentobler, U. (2013). On the importance of time and frequency in geodesy. In *2013 Joint European Frequency and Time Forum & International Frequency Control Symposium (EFTF/IFC)*. IEEE.

Schuldt, T., Gohlke, M., Oswald, M., Wüst, J., Blomberg, T., Döringshoff, K., Bawamia, A., Wicht, A., Lezius, M., Voss, K., Krutzik, M., Herrmann, S., Kovalchuk, E., Peters, A., and Braxmaier, C. (2021). Optical clock technologies for global navigation satellite systems. *GPS Solutions*, 25(83).

Selvan, K., Siemuri, A., Prol, F. S., Välisuo, P., Bhuiyan, M. Z. H., and Kuusniemi, H. (2023). Precise orbit determination of leo satellites: a systematic review. *GPS Solutions*, 27(4):178.

Surof, J., Poliak, J., Wolf, R., Macri, L., Mata Calvo, R., Blümel, L., Dominguez, P., Giorgi, G., Agazzi, L., Furthner, J., and Günther, C. (2022). Validation of kepler time and frequency transfer on a terrestrial range of 10.45km. pages 3662–3670.

Teunissen, P. and Montenbruck, O., editors (2017). *Springer Handbook of Global Navigation Satellite Systems*. Springer Handbooks. Springer International Publishing.

Wolf, P. and Petit, G. (1995). Relativistic theory for clock syntonization and the realization of geocentric coordinate times. *Astron. Astrophys*, 304:653–661.